Adducts of *o*-Silaborane With Water and Methanol

Lars Wesemann,*[a] Michael Trinkaus,[b] Yves Ramjoie,[b] Beate Ganter,[b] Ulli Englert,[b] and Jens Müller*[b]

Keywords: Silaboranes / Cluster compounds / Siloxanes / Silicon / Boranes

The synthesis of alkoxide adducts of *o*-silaborane $[(TMPDAH)_2][(Me_2Si_2B_{10}H_{10})_2O]$ (**3**) and $[TMPDAH][(Me_2Si_2B_{10}H_{10})OMe]$ (**4**) are presented (TMPDA = tetramethylpropylenediamine). For both silaborate clusters **3** and **4** the results of the NMR spectroscopic investigations together with the X-ray single crystal structure determinations are discussed. The geometries of ab initio calculations (HF and B3LYP methods) on the hydroxide adduct $[Si_2B_{10}H_{12}(OH)]^-$ are compared with the structures of **3** and **4**. The dynamic behaviour of the adducts **3** and **4** in solution is discussed with respect to the calculated energy profile for the rotation of the HSi(OH) group.

Introduction

Wade and Williams have developed a classification for borane and heteroborane clusters into groups of different numbers of skeleton electron pairs depending on the number of skeleton atoms.[1,2] On the basis of these rules the structure of a cluster with known composition can often be predicted. A *closo* cluster with n vertices can be transformed into a *nido* cluster by increasing the number of cluster electrons by two. The geometry of this *nido* cluster can be derived from the skeleton of the next higher *closo* cluster ($n + 1$ vertices). Figure 1 shows the thirteen vertex deltahedra and the three primary fragments that result from the removal of a single 4k, a selected 5k, and one of the 6k vertices.

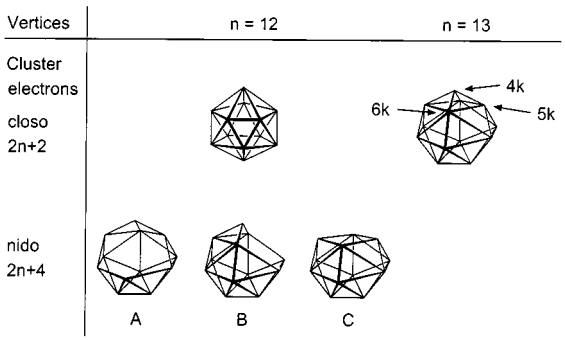

Figure 1. *closo* Clusters with 12 and 13 vertices and *nido* clusters with 12 vertices; in A the 6k vertex, in B the 5k vertex, and in C the 4k vertex is removed

Hawthorne et al. have found a cluster-opening reaction with the reduction of *o*-carborane (geometry A).[3] Examples for geometry B have been published by Paetzold et al. with the adducts of aza-*closo*-dodecaborane(12).[4] So far, 12-vertex *nido* clusters with geometry C, exhibiting a quadrangle as the open cluster face, are unknown.[1] However, *nido* 12-vertex clusters with a geometry other than the primary fragments are known. In the case of the fluxional tetracarbon cluster $R_4C_4B_8H_8$ a variety of cluster geometries has been determined by crystal structure analysis or NMR spectroscopy.[5–7] Depending on the substituents present at the carbon vertices, cluster skeletons exhibiting two neighboring quadrangles or a hexagonal open face have been characterized in the solid state. Adducts of *closo*-heterodicarbaboranes ($MC_2B_9H_{11}$ or $MC_2B_4H_6$) show opened-cluster frameworks, which have been considered as slip distorted geometries with respect to the central heteroatom.[8]

The reaction of the *commo*-cluster $[Si(C_2B_9H_{11})_2]$ with PMe_3 or pyridine results, in both cases, in an opened-cluster geometry.[9] Interestingly, the phosphane removes a boron vertex from the framework and pyridine attacks the silicon resulting in η^1-coordination of the silicon at the cluster.
The first studies on the nucleophilic degradation of 1,2-dimethyl-1,2-disila-*closo*-dodecaborane(12) (*o*-silaborane) (**1**)[10] have resulted in the isolation of a surprising adduct between the *closo*-cluster and dialkylamides.[11] Adducts of this type have been isolated in the case of dimethyl- and diphenyl-*o*-silaborane.[11,12] Regarding the cluster electron count of these adducts, an opened *arachno*-cluster geometry is expected according to the cluster rules. Surprisingly, the adducts show a structure which is closely related to the starting material and is not in agreement with Williams topological systematics (Scheme 1).

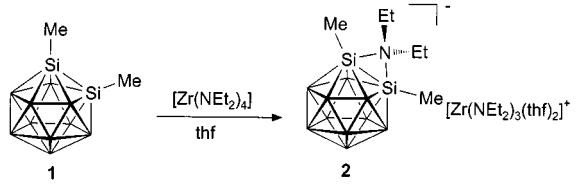

Scheme 1

The crystallographically determined structure and the NMR chemical shifts (^{11}B, ^{29}Si) of **1** and **2** have been repro-

[a] Institut für Anorganische Chemie, Universität zu Köln, Greinstraße 6, D-50939 Köln, Germany
[b] Institut für Anorganische Chemie der Technischen Hochschule Aachen, Prof.-Pirlet-Strasse 1, D-52056 Aachen, Germany

  1434–1948/00/0404–0735 $ 17.50+.50/0

duced by ab initio calculations. The LUMO of the *o*-silaborane should be responsible for the interesting acceptor abilities. This empty orbital is essentially concentrated on the two silicon atoms and shows bonding character with respect to the silicon–silicon distance. In order to get further insight into the acceptor abilities of *o*-silaborane we studied the reaction with other nucleophiles.

Results and Discussion

Synthesis, NMR Spectroscopy, and X-ray Diffraction Studies

In this publication we present oxide *o*-silaborane adducts exhibiting a hitherto unknown cluster geometry. By accident we found a reaction of the *closo*-silaborane with water. During our studies on the reactivity of the icosahedral cluster **1** towards tertiary amines, the remaining moisture in the inert gas was found to be the source of water. One equivalent of *o*-silaborane (**1**) reacts with water and one equivalent of tetramethylpropylenediamine (TMPDA) to give the oxide adduct **3** in quantitative yield (Scheme 2).

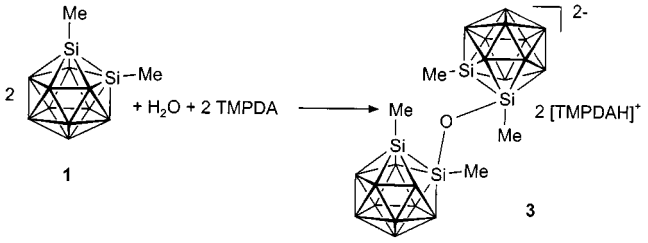

Scheme 2

The silaborane could be completely recovered after addition of aqueous HCl to a THF solution of the dianion **3**, indicating the reversibility of this acid-base reaction. Exclusion of water from the inert gas enabled us to introduce other less-acidic reagents into this reaction. Thus methanol reacts with TMPDA and one equivalent of *o*-silaborane to give the methoxide adduct **4** (Scheme 3). This adduct formation is also reversible, as is shown by the complete recovery of *o*-silaborane after acidification of a solution of the methoxide adduct **4**.

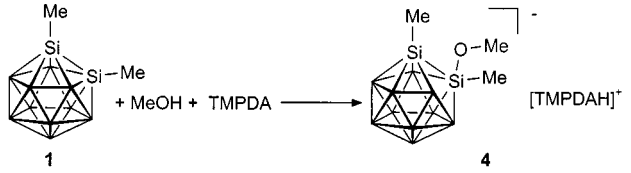

Scheme 3

Compounds **3** and **4** have been characterized by elemental analysis, multinuclear/multidimensional NMR spectroscopy, and X-ray structure analysis. In both cases crystals suitable for X-ray diffraction were obtained by slow diffusion of hexane into a THF solution of the salts **3** and **4**. Perspective views of the cluster anions of **3** and **4** are depicted in Figure 2 and Figure 3, respectively. Selected interatomic distances are listed in Table 1 and Table 2.

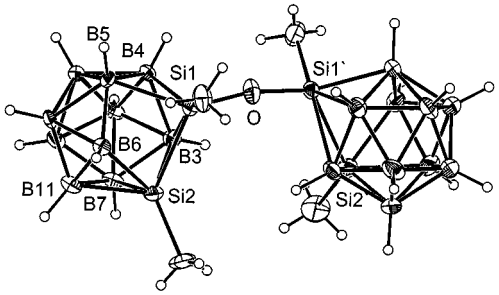

Figure 2. Structure of the anion of **3** in the crystal (PLATON representation,[16] ellipsoids at 30% probability level)

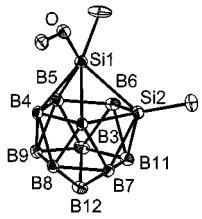

Figure 3. Structure of the anion of **4** in the crystal (PLATON representation,[16] ellipsoids at 30% probability level)

Table 1. Selected interatomic distances in the anion of **3** and **4** [Å]

	Anion of **3**	Anion of **4**
Si–Si	2.391(2), 2.374(2) 2.478(2), 2.364(2)	2.391(2)
Si1–O	1.629(3), 1.647(3) 1.643(4), 1.651(3)	1.674(3)
Si1–B3	2.255(6), 2.281(6) 2.229(6), 2.301(5)	2.254(5)
Si1–B4	2.076(6), 2.092(6) 2.081(5), 2.098(6)	2.081(5)
Si1–B5	2.172(5), 2.141(6) 2.119(6), 2.181(6)	2.126(6)
Si1–B6	2.458(6), 2.408(6) 2.395(6), 2.385(6)	2.400(6)
Si2–B3	2.064(6), 2.075(6) 2.035(6), 2.074(6)	2.082(6)
Si2–B6	2.056(4), 2.048(6) 2.005(5), 2.086(6)	2.040(6)
Si2–B7	2.055(6), 2.048(6) 2.044(6), 2.058(6)	2.051(5)
Si2–B11	2.068(6), 2.053(6) 2.021(6), 2.048(6)	2.060(6)

Table 2. Selected bond angles in the anion of **3** and **4** [°]

	Anion of **3**	Anion of **4**
Si2–Si1–O	120.3(1), 121.0(1) 156.8(1), 123.3(1)	125.0(1)
Si–O–Si	164.2(2), 154.6(2)	–
Si–O–C	–	132.3(3)
Si1–Si2–C2	127.4(3), 127.3(2) 123.4(3), 128.9(1)	126.6(2)
Si2–Si1–C1	114.1(3), 113.7(3) 87.7, 123.3(3)	109.1(3)
O–Si1–B12–B9	84.1(4), 87.2(3), 33.3(4), 98.4(4)	80.9(3)

Two equivalents of the salt $[(TMPDAH)_2][(Me_2Si_2B_{10}H_{10})_2O]$ (**3**) were found to crystallize independently in the asymmetric unit, thus allowing the interatomic parameters of two different Si–O–Si bridged clusters to be discussed. The variations of the Si–O–Si angles [Si1–O1–Si3 164.2(2), Si5–O2–Si7 154.6(2)] and the Si–O bond lengths [Si1–O1 1.629(3), Si3–O1 1.647(3), Si5–O2 1.643(3), Si7–O2 1.651(3)] in the two dianions suggests flexibility of this linkage. This phenomenon has been well-established by several structural and theoretical studies on molecules bear-

ing disiloxane moieties.[17] Thus, an increase in the Si–O–Si angle causes a decrease in the Si–O distance. The presented structural data of the oxide bridged silaboranes are in agreement with this tendency.

The cluster geometries of the oxide and methoxide adducts show a high degree of similarity. In both cases the Si–B distances are in the range of 2.3–2.0 Å. The longest distances between silicon and boron are found in each cluster between Si1, the silicon atom carrying the alkoxide, and B3, the boron atom which is still coordinated to both silicon atoms [2.254(5), 2.255(6), 2.281(6), 2.229(6), 2.301(5) Å]. This adduct formation is also a cluster-opening reaction. The silicon atom attacked by the nucleophile is coordinated to only three boron atoms. Obviously, the bond to the boron atom opposite to the entering nucleophile was broken during adduct formation (see Table 1 Si1–B6). Therefore, the adduct features a quadrangle consisting of two silicon atoms and two boron atoms (Type C in Figure 1). Overall the coordination number of Si1 remains as six. The silicon atom not attached to the oxygen atom is embedded in the cluster framework as in the starting material. The geometry of the oxygen adducts of *o*-silaborane can be derived from the 13-vertex *closo* skeleton by removal of the four-coordinate vertex (4k).

The static geometries of the silaborate derivatives **3** and **4** in the solid state are not compatible with the NMR spectroscopic studies at room temperature. Instead, the number of signals in the ^{1}H-, ^{11}B-, ^{13}C-, and ^{29}Si-NMR spectra equals the number observed for *o*-silaborane, possessing C_{2v} symmetry. A dynamic process involving migration of the oxygen between the neighboring silicon atoms accounts for the smaller number of signals than would be expected for the static compounds. This fluxional process is too rapid on the NMR time scale to be quenched at room temperature.

Ab Initio Calculations

In order to get further insights into the dynamic behavior we studied the oxygen adducts by ab initio calculations.[18] Instead of the anion of compound **4**, we conducted the calculations with the parent compound $[Si_2B_{10}H_{12}(OH)]^-$. Figure 4 shows the relative energies at the HF/6-31G(d) level dependent on the rotation of the SiH(OH) group (see Experimental Section). We chose Si1–B12 as the axis of rotation; i.e., we varied the O–Si1–B12–B9 (Figure 3) torsion angle in steps of 10° and optimized the resulting 19 geometries. We checked that Figure 4 describes an internal reaction path by frequency analyses. This surface scan (Figure 4) clearly shows two minima, **M1** and **M2**, and two transition states, **TS1** and **TS2**. Moreover, we conducted full optimizations for the two equilibrium geometries and the transition state highest in energy (**TS2**), both at the HF/6-31G(d) and the B3LYP/6-31G(d) levels of theory. The calculated structures are depicted in Figure 5 and selected bond lengths and additional data are compiled in Table 3.

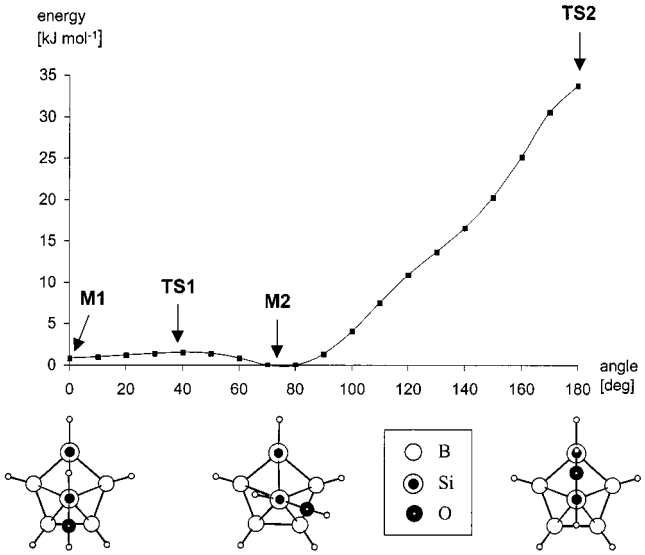

Figure 4. Surface scan for the rotation of the SiH(OH) group in $[Si_2B_{10}H_{12}(OH)]^-$ at the HF/6-31G(d) level

Besides **M1**, **M2**, and **TS2**, Figure 5 shows the two additional geometrical conformers, **M3** and **TS3**. The transition state **TS3** has the OH group symmetrically bound to both Si atoms (C_s point group). This transition state connects two enantiomers of **M3** (C_1 point group) and corresponds to an exchange of the OH group between the two Si atoms. The barrier for this process is only 29.9 kJ mol^{-1} [B3LYP/6-31G(d)].

The major difference between the structures of **M1**, **M2**, **TS1**, and **TS2** on the one side, and **M3** and **TS3** on the other, is the conformation of the OH group. Whereas for **M1**–**TS2** the H atom of the hydroxy group is directed towards the surface of the cluster (torsion angle H–O–Si1–B12 = 180°), for **M3** and **TS3** the H atom is directed in the opposite direction (Figure 5). Obviously, the two reaction coordinates **M1**–**TS1**–**M2**–**TS2** (Figure 4) and **M3**–**TS3** are related by the rotation of the OH group along the Si1–O bond. Therefore, we took several geometries from the surface scan of Figure 4 and rotated the OH group by 180° to give a new set of starting geometries. These optimizations led to two minima at the HF/6-31G(d) level which were similar to **M3**; i.e., 17.4 and 18.8 kJ mol^{-1} higher in energy than **M2**. The barrier for SiH(OH) rotation is just 30.7 kJ mol^{-1} at the B3LYP/6-31G(d) level (Figure 5).

The geometry corresponding to the minimum **M2**, and the structure of the anion of **4**, are very similar. In particular, the calculated and measured torsion angle O–Si1–B12–B9 is 75.3° (75.6°) and 80.9(3)°, respectively. The corresponding torsion angles of the two independent anions of **3** in the solid state are 84.1(4) and 87.2(3)° for one molecular unit, and 33.3(4) and 98.4(4)° for the other molecular unit. These torsion angles are in the flat region of the calculated surface (Figure 4) showing the high degree of flexibility.

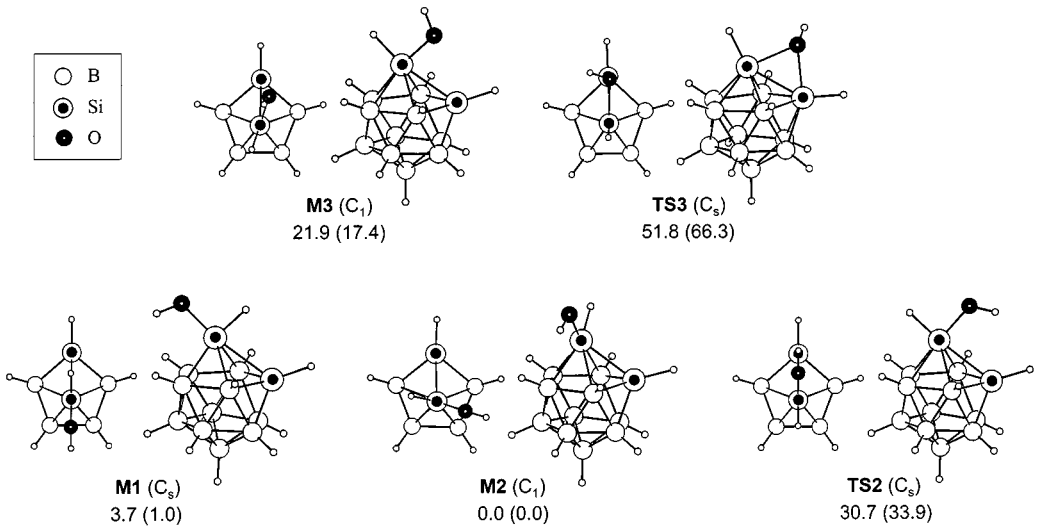

Figure 5. Minimum structures and transition states of $[Si_2B_{10}H_{12}(OH)]^-$; relative energies in kJ mol^{-1} at the B3LYP/6-31G(d) and the HF/6-31G(d) level (in parentheses); two views are depicted for each molecule

Table 3. Bond lengths in Å calculated at the B3LYP/6-31G(d) and the HF/6-31G(d) level (in parentheses)

	M1	M2	M3	TS2	TS3
Si1–Si2	2.492 (2.502)	2.377 (2.377)	2.422 (2.424)	2.461 (2.462)	2.329 (2.315)
Si1–O	1.706 (1.684)	1.708 (1.686)	1.732 (1.708)	1.723 (1.702)	1.996 (1.970)
Si1–B3	2.279 (2.278)	2.288 (2.283)	2.255 (2.257)	2.258 (2.250)	2.103 (2.102)
Si1–B4	2.082 (2.085)	2.112 (2.116)	2.077 (2.083)	2.107 (2.112)	2.066 (2.075)
Si1–B5	2.082 (2.085)	2.116 (2.123)	2.111 (2.116)	2.107 (2.112)	2.071 (2.079)
Si1–B6	2.279 (2.278)	2.391 (2.387)	2.199 (2.197)	2.258 (2.250)	2.111 (2.108)

The geometry corresponding to the transition state **TS3** compares well with the structure of the dimethylamide adduct **2** (Scheme 1).[11]

Experimental Section

General Considerations: All manipulations were carried out under an atmosphere of nitrogen using standard Schlenk techniques. THF was distilled from sodium/benzophenone, and hexane from potassium, and each was stored under nitrogen. – Elemental analyses were performed by the Mikroanalytisches Labor Pascher (Remagen) or the Analytischen Laboratorien (Lindlar). – NMR spectroscopy was performed on a Varian Unity 500 MHz spectrometer (^{1}H: 500 MHz, ^{11}B: 164 MHz, ^{13}C: 125 MHz, ^{29}Si: 100 MHz).

[(TMPDAH)$_2$][(Me$_2$Si$_2$B$_{10}$H$_{10}$)$_2$O] (3): A solution of **1** (264.2 mg, 1.29 mmol) in THF (15 mL) was treated with TMPDA (1.0 g, 7.68 mmol) and H_2O (0.015 mL, 0.94 mmol). The colorless solution was stirred overnight. All volatiles were removed and the remaining colorless solid was characterized by NMR spectroscopy to be almost quantitatively **3**. Crystalline material was obtained by slow diffusion of hexane into a THF solution of **3** (Yield: 426 mg, 0.62 mmol, 96%). – ^{1}H{^{11}B} NMR (500 MHz, TMS, CD_2Cl_2): δ = 0.84 (s, 6 H, SiCH_3), 1.25 (s, 2 H, H9/12), 1.39 (s, 2 H, H4/5/7/11), 1.67 (s, 2 H, H8/10), 1.86 (quin., 2 H, NCH$_2$CH_2CH$_2$N), 1.86 (s, 2 H, H3/6), 2.59 (s, 12 H, NCH_3), 2.98 (t, 4 H, NCH_2CH$_2$CH_2N), 11.19 (s, 1 H, N*H*N). – ^{11}B NMR (160 MHz, $BF_3 \cdot Et_2O$): δ = –11.6 (d, ^1J = 122 Hz, B3/6), –14.5 (d, ^1J = 134 Hz, B8/10), –17.3 (d, ^1J = 122 Hz, B4/5/7/11), –21.1 (d, ^1J = 122 Hz, B9/12). – ^{13}C{^{1}H} NMR (125.6 MHz, TMS): δ = 6.6 (MeSi), 21.7 (s, NCH$_2$*C*H$_2$CH$_2$N), 44.7 [s, N(CH$_3$)$_2$], 60.1 (s, N*C*H$_2$CH$_2$*C*H$_2$N). – ^{29}Si NMR (MHz, TMS): δ = –73.7. – $C_{18}H_{70}B_{20}N_4OSi_4$ (687.35): calcd C 31.46, H 10.27, N 8.15, O 2.33; found C 31.27, H 10.51, N 8.03, O 2.12.

X-ray Crystallographic Analysis of 3: $C_{18}H_{70}B_{20}N_4OSi_4$, ENRAF-Nonius CAD4; Mo-$K_\alpha$ radiation, λ = 0.71073 Å, graphite monochromator; data collection with ω-2θ scan at 203 K, Colorless translucent platelet 0.7 × 0.5 × 0.1 mm, triclinic space group $P\bar{1}$ (no. 2); a = 8.451(2), b = 22.697(3), c = 22.992(3) Å, α = 97.42(1), β = 100.01(1), γ = 100.32(1)°, U = 4214(1) Å^3, Z = 4, ρ_{calcd} = 1.083 gcm^{-3}, μ(Mo-K_α) = 1.60 cm^{-1}, F(000) = 1480; 15805 reflections in the range 2 < θ < 26°, 15226 independent reflections. Structure solution by direct methods[13] and refinement[14] on F^2 for 1366 variables; all nonhydrogen atoms refined isotropically. Convergence at R = 0.074 for 7172 observations with $F_o > 4\sigma F_o$, $wR2$ = 0.154 for all reflections, $w^{-1} = \sigma^2(F_o^2) + \{0.052[\max(F_o^2,0) + 2F_c^2]/3\}^2$, GOF = 0.929.

[TMPDAH][(Me$_2$Si$_2$B$_{10}$H$_{10}$)OMe] (4): A solution of **1** (330.0 mg, 1.61 mmol) in THF (15 mL) was treated with TMPDA (255.3 mg, 1.21 equiv.). After stirring for 30 min CH_3OH (55 mg, 1.07 equiv.) was added. The colorless solution was stirred overnight. All volatiles were removed and the remaining colorless solid was characterized by NMR spectroscopy to be almost quantitatively **4**. Crystalline material was obtained after slow diffusion of hexane into a THF solution of **4** (yield: 572 mg, 1.56 mmol, 97%). – ^{1}H{^{11}B} NMR (500 MHz, TMS, THF): δ = 0.76 (s, 6 H, SiCH_3), 1.22 (s, 2 H, H9/12), 1.37 (s, 4 H, H4/5/7/11), 1.72 (s, 4 H, H3/6/8/10), 1.88 (quin., 2 H, NCH$_2$CH_2CH$_2$N), 2.61 (s, 12 H, NCH_3), 2.97 (t, 4 H, NCH_2CH$_2$CH_2N), 11.04 (s, 1 H, N*H*N). – ^{11}B NMR (160 MHz, $BF_3 \cdot Et_2O$): δ = –13.8 (d, ^1J = 140 Hz, B3/6/8/10), –17.5 (d, ^1J = 128 Hz, B4/5(7/11), –20.5 (d, ^1J = 128 Hz, B9/12). – ^{13}C{^{1}H} NMR (125.6 MHz, TMS): δ = 3.6 (MeSi), 21.2 (NCH$_2$*C*H$_2$CH$_2$N), 44.5 [–N(*C*H$_3$)$_2$], 60.2 (N*C*H$_2$CH$_2$*C*H$_2$N). – ^{29}Si NMR (MHz, TMS): δ = –69.3. – $C_{10}H_{38}B_{10}N_2OSi_2$ (366.71): calcd C 32.75, H 10.45, N 7.64; found C 32.53, H, 10.24, N 7.79.

X-ray Crystallographic Analysis of 4: $C_{10}H_{38}B_{10}N_2OSi_2$, ENRAF-Nonius CAD4; Cu-$K_\alpha$ radiation, $\lambda = 1.54184$ Å, graphite monochromator; data collection with ω-2θ scan at 180 K. Colorless platelet $0.36 \times 0.24 \times 0.08$ mm, monoclinic space group $P2_1/c$ (no. 14); $a = 8.808(1)$, $b = 9.139(1)$, $c = 28.218(7)$ Å, $\beta = 94.24(2)°$, $U = 2265.(1)$ Å^3, $Z = 4$, $\rho_{calcd} = 1.078$ gcm^{-3}, μ(Cu-K_α) = 14.10 cm^{-1}, $F(000) = 792$; 5639 reflections in the scan range $4 < \theta < 70°$, 2599 independent observations with $I > \sigma(I)$ in structure solution with direct methods[13] and refinement[15] on F for 306 variables; all nonhydrogen atoms refined with anisotropic replacement parameters, hydrogen atoms refined isotropically. Convergence at $R = 0.066$, $Rw = 0.063$, $w^{-1} = \sigma^2(F_o)$, $GOF = 1.094$.

Crystallographic data (excluding structure factors) for the structures reported in this paper have been deposited with the Cambridge Crystallographic Data Centre as supplementary publication nos. CCDC-114742 (**3**) and CCDC-114741 (**4**). Copies of the data can be obtained free of charge on application to CCDC, 12 Union Road, Cambridge CB2 1EZ, UK [Fax: (internat.) +44–1223/336-033; E-mail: deposit@ccdc.cam.ac.uk].

Ab Initio Calculations: The Gaussian 94 package,[18] run on a cluster of workstations (*Rechenzentrum der RWTH Aachen*), was applied for all ab initio calculations. The calculations were conducted in redundant internal coordinates. The surface scan of Figure 4 was performed by a step-by-step change of the torsion angle O–Si1–B12–B9 by 10° followed by an optimization of all other geometrical parameters. All full geometry optimizations were conducted without any symmetry restrictions (Figure 5). The total energies E_h (in Hartrees; B3LYP/6-31G(d) and HF/6-31G(d) in parentheses) and ZPVE calculated at HF/6-31G(d) level (in kJ mol^{-1}; in square brackets) are as follows: **M1**: –910.812603 (–907.220984) [483.2], **M2**: –910.814022 (–907.221375) [483.4], **M3**: –910.805689 (–907.214743) [482.1], **TS2**: –910.802310 (–907.208467) [481.8], **TS3**: –910.794274 (–907.196112) [481.4].

Acknowledgments

We are grateful to the Deutsche Forschungsgemeinschaft (DFG-Schwerpunktprogramm "Polyeder") for generous financial support and to the Rechenzentrum der RWTH Aachen for providing generous computer time. Especially, we would like to thank T. Eifert and J. Risch for their support.

[1] K. Wade, *Adv. Inorg. Chem. Radiochem.* **1976**, *18*, 1–66.
[2] R. E. Williams, *Advances in Boron Chemistry* (Ed.: W. Siebert), The Royal Society of Chemistry, Cambridge, **1997**; R. E. Williams, *Adv. Inorg. Chem. Radiochem.* **1976**, *18*, 67–105.
[3] T. D. Getman, C. B. Knobler, M. F. Hawthorne, *Inorg. Chem.* **1990**, *29*, 158–160.
[4] F. Meyer, J. Müller, P. Paetzold, R. Boese, *Angew. Chem*. **1992**, *104*, 1221–1222; *Angew. Chem. Int. Ed.* **1992**, *31*, 1227–1228.
[5] [5a] R. N. Grimes, *Adv. Inorg. Chem. Radiochem.* **1983**, *26*, 55–117; [5b] R. N. Grimes, *Coord. Chem. Rev.* **1995**, *143*, 71–96.
[6] D. P. Freyberg, R. Weiss, E. Sinn, R. N. Grimes, *Inorg. Chem*. **1977**, *16*, 1847–1851.
[7] R. N. Grimes, W. N. Maxwell, R. B. Maynard, E. Sinn, *Inorg. Chem.* **1980**, *19*, 2981–2985.
[8] A. K. Saxena, J. A. Maguire, N. S. Hosmane, *Chem. Rev.* **1997**, *97*, 2421–2461.
[9] D. M. Schubert, W. S. Rees, Jr. C. B. Knobler, M. F. Hawthorne, *Organometallics* **1990**, *9*, 2938–2944.
[10] L. Wesemann, U. Englert, D. Seyferth, *Angew. Chem.* **1995**, *107*, 2435–2436; *Angew. Chem. Int. Ed. Engl.* **1995**, *34*, 2236–2238.
[11] L. Wesemann, Y. Ramjoie, M. Trinkaus, B. Ganter, J. Müller, *Angew. Chem*. **1998**, *110*, 1481–1484; *Angew. Chem. Int. Ed.* **1998**, *37*, 1412–1415.
[12] L. Wesemann, Y. Ramjoie, M. Trinkaus, B. Ganter, *Z. Allg. Anorg. Chem.* **1998**, 624, 1573–1576.
[13] G. M. Sheldrick, *SHELXS86, Program for Structure Solution*, University of Göttingen, Germany, **1986**.
[14] G. M. Sheldrick, *SHELXS93, Program for Structure Refinement*, University of Göttingen, Germany, **1993**.
[15] B. A. Frenz and ENRAF-Nonius, SDP, Version 5.0 (**1989**).
[16] A. L. Spek, *Acta Crystallogr. Sect. A* **1990**, *46*, C34.
[17] F. Cervantes-Lee, H. K. Sharma, K. H. Pannell, A. Derecskei-Kovacs, D. S. Marynick, *Organometallics* **1998**, *17*, 3701–3706; K. M. Baines, A. G. Brooks, P. D. Lickiss, J. F. Sawyer, *Organometallics* **1989**, *8*, 709–716.
[18] All calculations were performed with Gaussian 94, M. J. Frisch, G. W. Trucks, H. B. Schlegel, P. M. W. Gill, B. G. Johnson, M. A. Robb, J. R. Cheeseman, T. Keith, G. A. Petersson, J. A. Montgomery, K. Raghavachari, M. A. Al-Laham, V. G. Zakrzewski, J. V. Ortiz, J. B. Foresman, J. Cioslowski, B. B. Stefanov, A. Nanayakkara, M. Challacombe, C. Y. Peng, P. Y. Ayala, W. Chen, M. W. Wong, J. L. Andres, E. S. Replogle, R. Gomperts, R. L. Martin, D. J. Fox, J. S. Binkley, D. J. Defrees, J. Baker, J. P. Stewart, M. Head-Gordon, C. Gonzalez, J. A. Pople, Gaussian, Inc., Pittsburgh PA, **1995**.

Received August 10, 1999
[I99294]